Eur J Nucl Med Mol Imaging (2008) 35:1681–1691
DOI 10.1007/s00259-008-0808-z

ORIGINAL ARTICLE

Metabolic connectivity by interregional correlation analysis using statistical parametric mapping (SPM) and FDG brain PET; methodological development and patterns of metabolic connectivity in adults

Dong Soo Lee · Hyejin Kang · Heejung Kim · Hyojin Park · Jungsu S. Oh · Jae Sung Lee · Myung Chul Lee

Received: 23 December 2007 / Accepted: 5 April 2008 / Published online: 20 May 2008

Abstract
Purpose Regionally connected areas of the resting brain can be detected by fluorodeoxyglucose-positron emission tomography (FDG-PET). Voxel-wise metabolic connectivity was examined, and normative data were established by performing interregional correlation analysis on statistical parametric mapping of FDG-PET data.
Materials and methods Characteristics of seed volumes of interest (VOIs) as functional brain units were represented by their locations, sizes, and the independent methods of their determination. Seed brain areas were identified as population-based gyral VOIs (n=70) or as population-based cytoarchitectonic Brodmann areas (BA; n=28). FDG uptakes in these areas were used as independent variables in a general linear model to search for voxels correlated with average seed VOI counts. Positive correlations were searched in entire brain areas.
Results In normal adults, one third of gyral VOIs yielded correlations that were confined to themselves, but in the others, correlated voxels extended to adjacent areas and/or contralateral homologous regions. In tens of these latter areas with extensive connectivity, correlated voxels were found across midline, and asymmetry was observed in the patterns of connectivity of left and right homologous seed VOIs. Most of the available BAs yielded correlations reaching contralateral homologous regions and/or neighboring areas. Extents of metabolic connectivity were not found to be related to seed VOI size or to the methods used to define seed VOIs.
Conclusions These findings indicate that patterns of metabolic connectivity of functional brain units depend on their regional locations. We propose that interregional correlation analysis of FDG-PET data offers a means of examining voxel-wise regional metabolic connectivity of the resting human brain.

Keywords Interregional correlation analysis · Metabolic connectivity · Probabilistic map · FDG-PET

Electronic supplementary material The online version of this article (doi:10.1007/s00259-008-0808-z) contains supplementary material, which is available to authorized users.

D. S. Lee (✉) · H. Kang · H. Kim · H. Park · J. S. Oh · J. S. Lee · M. C. Lee
Department of Nuclear Medicine, Seoul National University, College of Medicine,
28 Yeongeon-dong,
Jongno-gu, Seoul 110–744, Korea
e-mail: dsl@plaza.snu.ac.kr

H. Kang
Programs in Brain and Neuroscience,
Seoul National University,
Seoul, Korea

H. Kim · H. Park
Interdisciplinary Program in Cognitive Science,
Seoul National University,
Seoul, Korea

Introduction

Long-distance brain circuit interactions are being actively investigated using various methods. The resting default-mode of the brain was first presumed to explain the resting deactivation of midline structures and lateral parietal lobes on water/oxygen positron emission tomography (PET) by Raichle et al. [1] and was later successfully utilized in

another resting-state functional magnetic resonance imaging (fMRI) network analysis study [2]. In these studies, the existence of resting connected circuits was assumed, and the focus was placed on their disclosure. Subsequent studies using resting fMRI [3–7] or water PET have repeatedly reported resting brain circuits [8]. The present study provides an alternative method for examining metabolic connectivity based on voxel-wise interregional correlation analysis (IRCA) of statistical parametric mapping (SPM) using resting fluorodeoxyglucose (FDG)-PET data using population-based gyral or cytoarchitectonic seed brain regions. Resting brain circuits without task-related activities [9, 10] were presumed to be as identifiable by resting FDG-PET, as they are by resting-only fMRI or resting water PET.

Brain networks or circuitries of brain regions are referred to as being functionally or effectively connected [11, 12], and have been investigated by correlation, coherence, or component analyses using functional brain images [3, 7, 9, 13]. Resting components (weighted distributions of brain parts) or regions are assumed to be responsible for the brain's resting functions [2] and their deactivations; attenuations or the emergences of other brain components are supposed to explain brain performance at various distinct stages of cognition [4, 9, 10]. Interregional correlations of FDG uptakes represent summations of resting states in the human brain. During resting state FDG uptake, brain sensory inputs are available, while thought processes are supposedly involved in self-recognition, introspection, and/or drifting regardless of the environmental inputs.

Brain regions may be involved in one activity or multiple activities [14, 15]. To define seed volumes of interest (VOIs), parcellation presents the issue of bias with respect to the use of functional localizers [14, 16]. In the present study, we presume that anatomical localizers are good alternatives for functional localizers [17]. Gyral/sulcal patterns [18] and cytoarchitectonic part-maps [19] offer two standard methods of anatomical brain parcellation, whereby individual subject's differences are managed by the probabilistic construction of VOIs based on population brain-image data [20]. Moreover, if predefined VOIs are used to search for brain circuits, modeling using centers of masses of functional localizers, its justification, and the general post hoc problem of statistical inference can be overcome [4, 8, 21].

We adopted probabilistic VOIs acquired from a population by high-resolution MRI [17, 20] and microscopic cytoarchitectural studies [19]. Seventy VOIs (e.g., the superior, middle, and inferior frontal gyri) and the presently available 28 VOIs (e.g., Brodmann areas [BA] 17 [22], 41 [23], 44, 45 [24] were used as seed VOI variables for interregional correlation analyses. Recently, a general linear model has been described that correlates voxel counts of entire brains with weighted FDG uptakes of seed VOIs [25, 26]. This method is similar in concept but superior in objectiveness to the pioneering works of Horwitz et al. [8, 27–30], which predated the SPM era and depended on manual or template-based VOI definitions. Using IRCA and FDG-PET regional activities, we assumed that steady-state neuronal macro-connectivity can be approximated to the extent of interregional neurotransmitter-information transfer.

A spectrum of interregional correlations of metabolic activities was revealed during the present study. To validate the devised method, we excluded the possibilities that these correlations were simply artifacts related to VOI sizes or due to different methods of defining seed VOIs. Patterns of interregional correlations between seed brain areas during the resting state in normal adult human brains were characterized and classified. The implications of metabolic connectivity by FDG brain PET are discussed in the context of opinions voiced concerning resting default mode function/circuitry as revealed by resting fMRI. In this investigation, normative data of interregional metabolic connectivity was established using the devised IRCA and FDG-PET.

Materials and methods

Subjects Study subjects were recruited to draft a population-based probabilistic atlas of the Korean people [31], and population-based PET controls were added. Accordingly, 50 normal healthy adults (mean age: 37.8±11.7 years; range from 19 to 55 years old; men/women=28/22) were finally included. Study subjects had no history of any neurological, psychiatric or significant medical illness, or of substance abuse and were recruited from the local community via the Health Promotion Center at Seoul National University Hospital or using newspaper advertisements. Subjects were screened using the Korean version of the modified Mini-Mental State Exam, Mood Evaluation Scale and a simplified version of the handedness test.

FDG-PET image acquisition All subjects underwent PET scans once in the resting state. PET images were acquired using an ECAT Exact PET scanner (CTI-Siemens, Knoxville, USA). Axial and in-plane resolutions were 4.3 and 6.1 mm, respectively. Before FDG injection, a transmission scan was performed using three Ge-68 rod sources to obtain attenuation maps. Forty minutes after administering 370 MBq of F-18-FDG intravenously, emission images were acquired over a 20-min period. During this period, subjects lay still in a dimly lit room with eyes open and ears unplugged. Emission images were reconstructed in a 128×128×47 matrix with a pixel size of 2.1×2.1×3.4 mm using a filtered back projection method and a Shepp filter with a cutoff value of 0.35 cycles/pixel. All reconstructed images were corrected for attenuation.

Imaging analysis PET images were spatially normalized to the Korean standard PET template of young male adult subjects [20, 31] after conversion to Analyze format. To generate the PET template, MRI of 35 young male subjects were spatially normalized by linear transformation to a target MRI with average global shape, and the normalization parameters were reapplied to corresponding PET images. Transformed PET images were then averaged to produce the standard template. The Korean Statistical Probabilistic Anatomical Map (K-SPAM) was used whose production method was detailed in [17]. FDG mean counts of VOIs were extracted using Korean structural probabilistic maps for 70 brain regions using an in-house program (Fig. 1, [17, 20]), and 28 of cytoarchitectonic VOIs, which were transferred elastically to the Korean standard brain from the Caucasian template created by the Forschungszentrum Juelich group (Fig. 2. courtesy of Professors Zilles and Amunts). To obtain a probability-weighted mean count for each seed VOI, probability weighted sums of all voxel values in VOIs on FDG-PET images were divided by the sum of voxel probabilities following equation:

$$\frac{\sum_{i,j,k} I_{i,j,k} \times P_{i,j,k}}{\sum_{i,j,k} P_{i,j,k}}$$

where $I_{i,\ j,\ k}$ and $P_{i,\ j,\ k}$ are the voxel count of FDG-PET image and probabilistic map (K-SPAM) at the $(i,\ j,\ k)$th pixel, respectively.

These counts were globally normalized with respect to individual gray matter mean counts. All normalized images were smoothed using a 16-mm full width at half maximum Gaussian kernel to increase the signal-to-noise ratio.

For IRCA, extracted mean regional VOI counts were used as covariate to find regions showing significant (corrected $P<0.05$) voxel-wise correlations (simple linear regression, number of data points=50) across scans (subjects) using SPM2 (Wellcome Department of Cognitive Neurology,

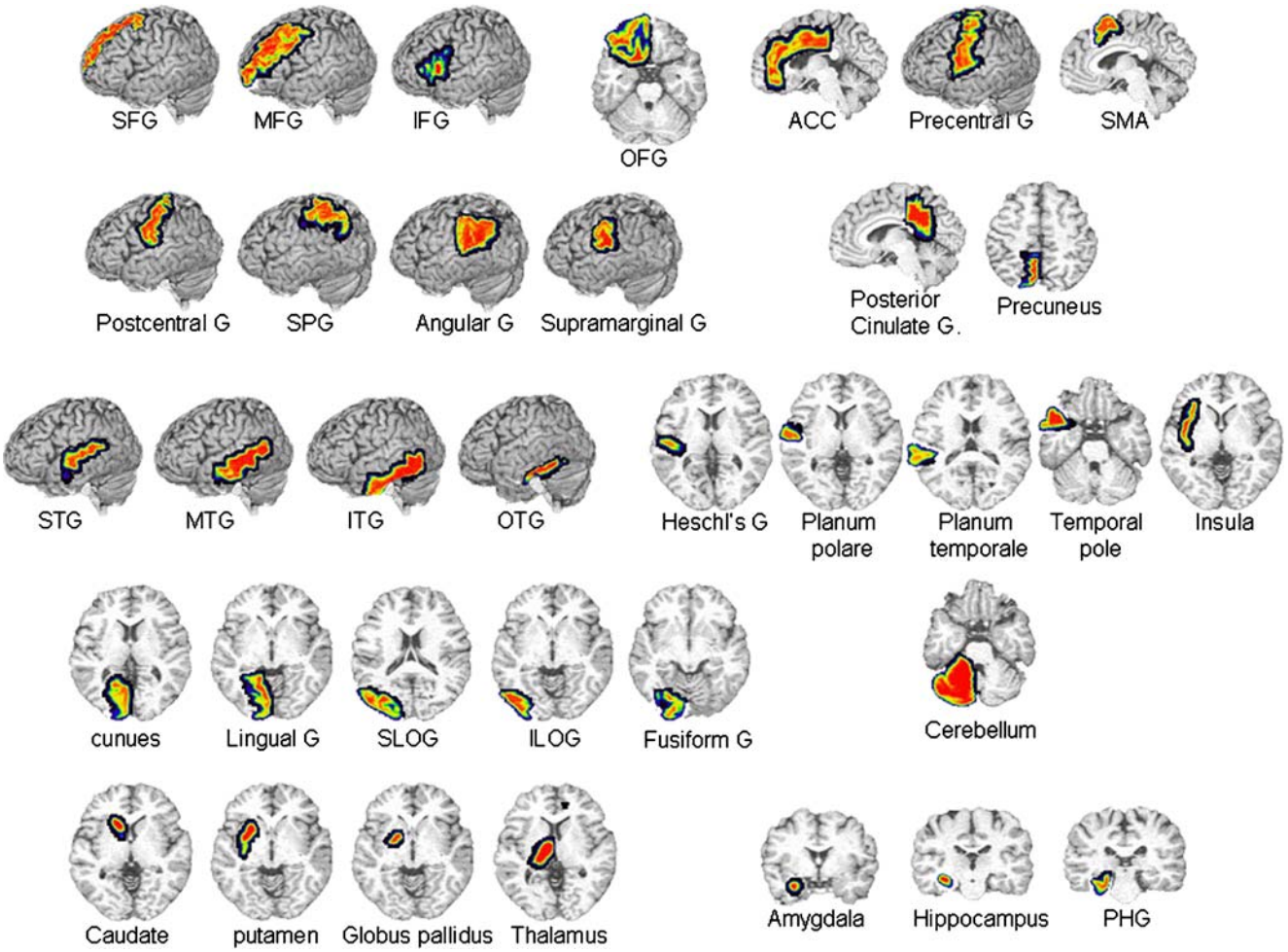

Fig. 1 Population-based probabilistic gyral VOIs on Korean brain templates. *G* gyrus, *SFG* superior frontal gyrus, *MFG* middle frontal gyrus, *IFG* inferior frontal gyrus, *OFG* orbitofrontal gyrus, *ACC* anterior cingulate cortex, *SMA* supplementary motor area, *SPG* superior parietal gyrus, *STG* superior temporal gyrus, *MTG* middle temporal gyrus, *ITG* inferior temporal gyrus, *OTG* occipitotemporal gyrus, *SLOG* superior lateral occipital gyrus, *ILOG* inferior lateral occipital gyrus, *PHG* parahippocampal gyrus

London) implemented in Matlab 6.5 (Mathworks, MA, USA; Fig. 3). To study asymmetries in interregional correlation patterns between the homologous counterparts of both hemispheres, we flipped images and used the *t*-test to determine asymmetries of areas of connectivity. Uncorrected *P* values of <0.001 were used to designate VOIs whose interregional correlation patterns differed from those of corresponding regions in contralateral hemispheres.

Each lobe was produced by summing the gyral probabilities, and mean lobe FDG counts were used as covariates to identify whole brain voxel-wise correlations. Sizes of seed VOIs were measured using the areas over 10% of probability (10–100%; Suppl Table 1). Sizes of correlated areas were defined as areas above threshold (corrected $P<0.05$), minus seed VOI areas. Size ratios of correlated areas per seed VOI were calculated by dividing correlated area sizes by seed VOI sizes. To evaluate the effect of VOI size on correlation extent, sizes of correlated areas or size ratios were compared with seed VOI sizes.

Results

Correlations confined to voxels within seed VOIs

All 70 (35 left and 35 right) gyral VOIs, defined on MR images, and all available 28 probabilistic BA, which were defined cytoarchitectonically, showed 'autocorrelation'.

We defined 'autocorrelation' as a correlation pattern in a given seed VOI that affected all or some of the voxels of the VOI and 'autocorrelation only' as a form of 'autocorrelation' that does not extend substantially beyond adjacent voxels and affect other VOIs. Thus, autocorrelation means that the voxels within seed VOIs were correlated with the weighted-mean FDG count of seed VOIs.

Patterns of correlation for gyral seed VOIs

Interregional correlations for 70 gyral VOIs ranged from autocorrelation only to interregional correlation with adjacent/remote areas including autocorrelation. Interregional correlation ranged from the immediate vicinities of seed VOIs to even remote areas across midline and contralateral homologues. Figure 4a illustrates the spectrum of outreaching patterns of interregional correlations. Green depicts seed VOIs showing 'autocorrelation only', yellow VOIs showing correlations reaching contralateral homologues, and red autocorrelation and wider areas of correlation with contralateral homologues and other regions. Suppl. Fig. 1 shows a number of gyral seed VOIs that demonstrate these three patterns of correlation.

Twenty-three of the 70 gyral VOIs showed 'autocorrelation only'. These seed VOIs were amygdala, hippocampus, parahippocampal gyrus, planum polare, Heschl's gyrus (Fig. 5a; Suppl. Fig. 2 transaxial display), planum temporale, superior, middle and inferior temporal gyri, occipitotemporal gyrus, and inferolateral occipital gyrus of both hemispheres. The left insula showed 'autocorrelation only' (Table 1).

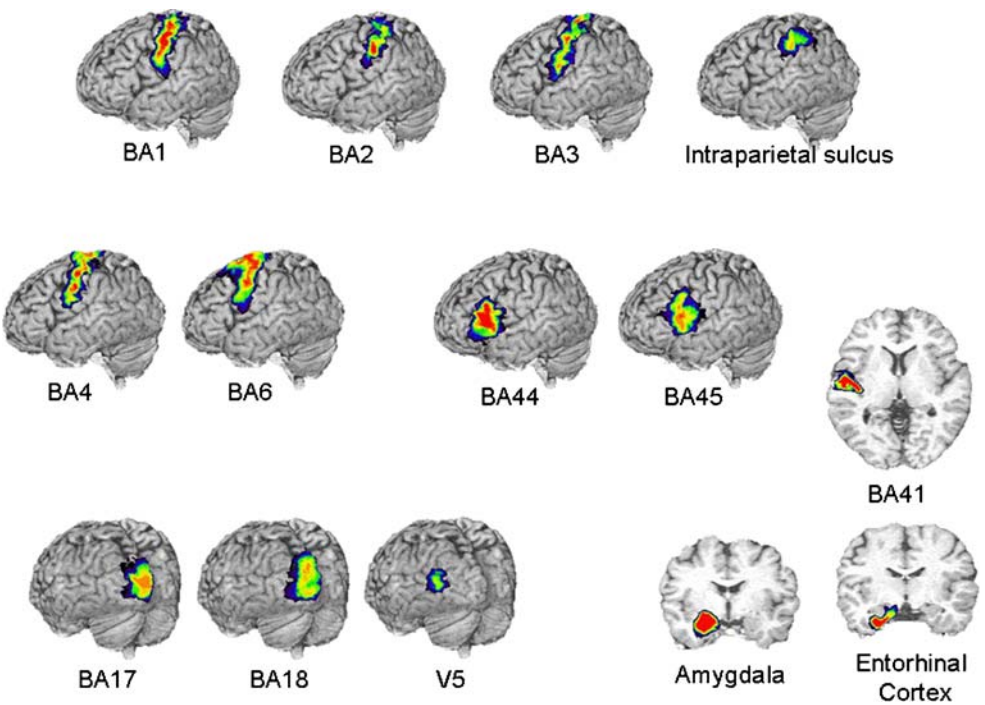

Fig. 2 BA on the Korean brain templates. Each BA was elastically transferred from the normative Caucasian to the normative Korean brain. The original BA were parceled using cytoarchitectonic methods, as previously described by Amunts and Zilles [19]. Regions of noncolored brain do not indicate a lack of connectivity, rather they indicate that cytoarchetectonic BA maps are not available. BA1, 2, and 3 [43, 44], BA4 and 6 [45], BA17 and 18 [22], V5 [46], BA41 [23], BA44 and BA45 [24], intraparietal sulcus [47], and amygdala and entorhinal cortex [48]

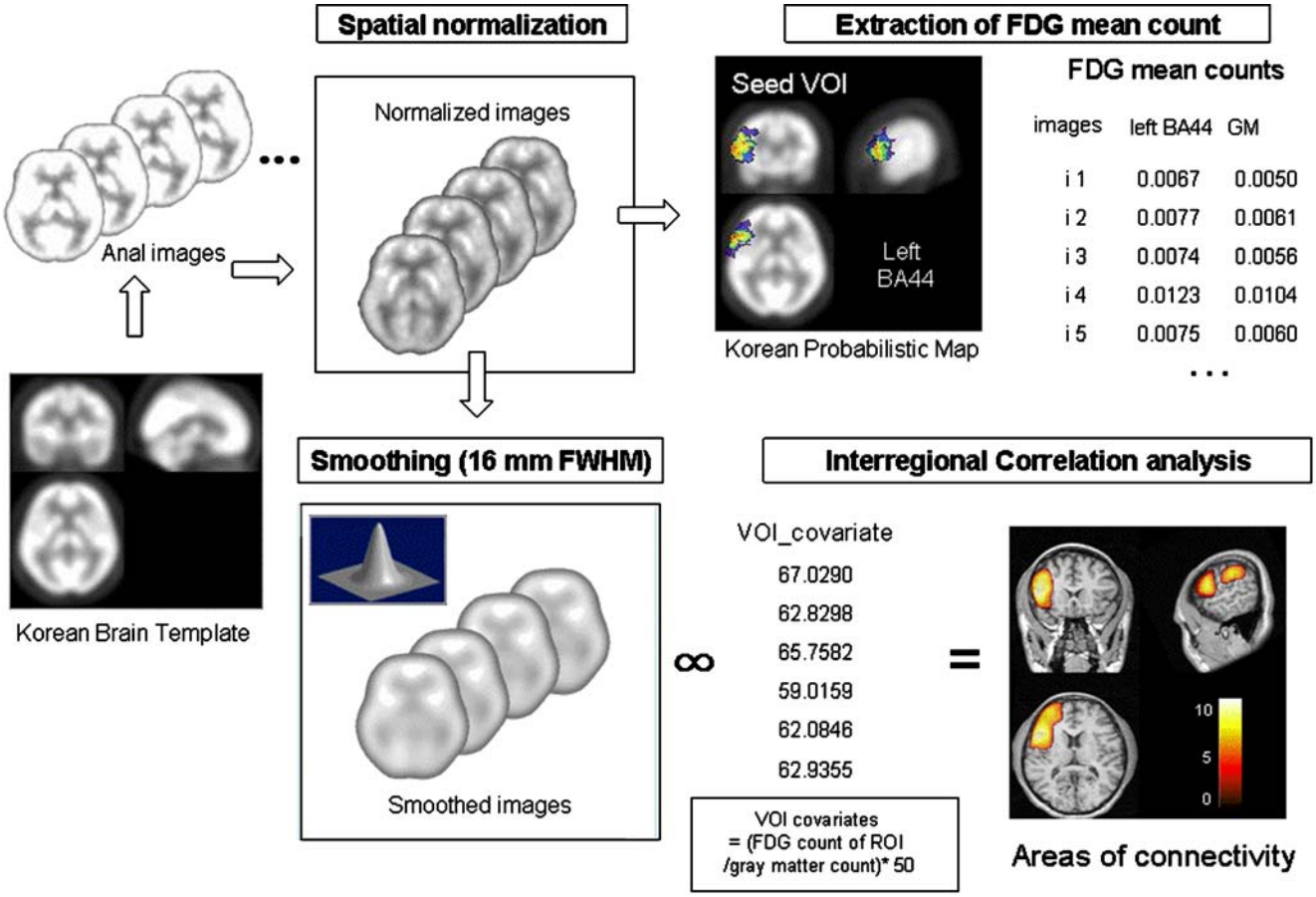

Fig. 3 IRCA/FDG-PET. All images were spatially transformed to the template brain and seed VOIs were determined on these normalized images. Normalized FDG counts of seed VOIs were calculated using the probability-weighted mean count method (see text). Seed VOI counts were then count normalized and used as a covariate in a general linear model of SPM2 to identify voxels showing significant correlations over individual brains ($P<0.05$ [corrected]; number of data points=50)

These 23 seed VOIs were characterized by the absence of a correlation with contralateral homologues.

For almost all of the remaining 47 gyral VOIs, correlations included homologous counterparts in contralateral hemispheres. Furthermore, 26 of these 47 gyral VOIs showed correlation only with all or parts of contralateral homologues (Suppl. Fig. 1). These were cerebellum, thalamus, putamen (Fig. 5b; Suppl. Fig. 3 for transaxial display), caudate, globus pallidus, cuneus, fusiform gyrus, lingual gyrus, superior lateral occipital gyrus, supramarginal gyrus, angular gyrus, temporal pole, and superior bilateral frontal gyri. In the other 21 gyral VOIs, correlation is more widely distributed, and these also included contralateral homologues (Suppl. Fig. 1). These other gyral VOIs were anterior and posterior cingulate gyri, postcentral gyrus, superior parietal gyrus, precuneus, middle and inferior frontal gyri, orbitofrontal gyrus, precentral gyrus (Suppl. Fig. 4), supplementary motor area of both hemispheres, and right insula.

Precentral and postcentral gyri and middle and inferior frontal gyri and insula showed hemispheric asymmetry between patterns of the areas correlated with homologous seed VOIs of both hemispheres.

Patterns of correlation for cytoarchitectonic seed VOIs

Of the available cytoarchitectonic VOIs (courtesy of Professors Amunts and Zilles of Insitut fuer Medizin, Forschungszentrum Juelich, Germany), 28 VOIs in both hemispheres were used as seed BA VOIs. Amygdala and BA41 (primary auditory cortex) in both hemispheres showed 'autocorrelation only' (Table 2).

Except for these VOIs, the remaining 24 VOIs in both hemispheres showed interregional correlations with wider areas. Twenty of these 24, BA1, BA2, BA3 (primary sensory cortices), BA4 (primary motor cortex), BA6 (premotor cortex), BA17 (visual area V1), BA18 (V2), anterior intraparietal sulcus, entorhinal cortex, and V5 in both hemispheres showed correlation with contralateral homologues and adjacent areas. BA44 (Fig. 5c; Suppl. Fig. 5 for transaxial display) and BA45 of both hemispheres showed wider areas of correlation in ipsilateral hemispheres but not with contralateral counterparts (Table 2). Asymmetry between left and right seed VOIs in terms of areas of correlation was found for BA44, BA45, and V5. Figure 4b shows the extents of interregional correlations shown by cytoarchitectonic seed

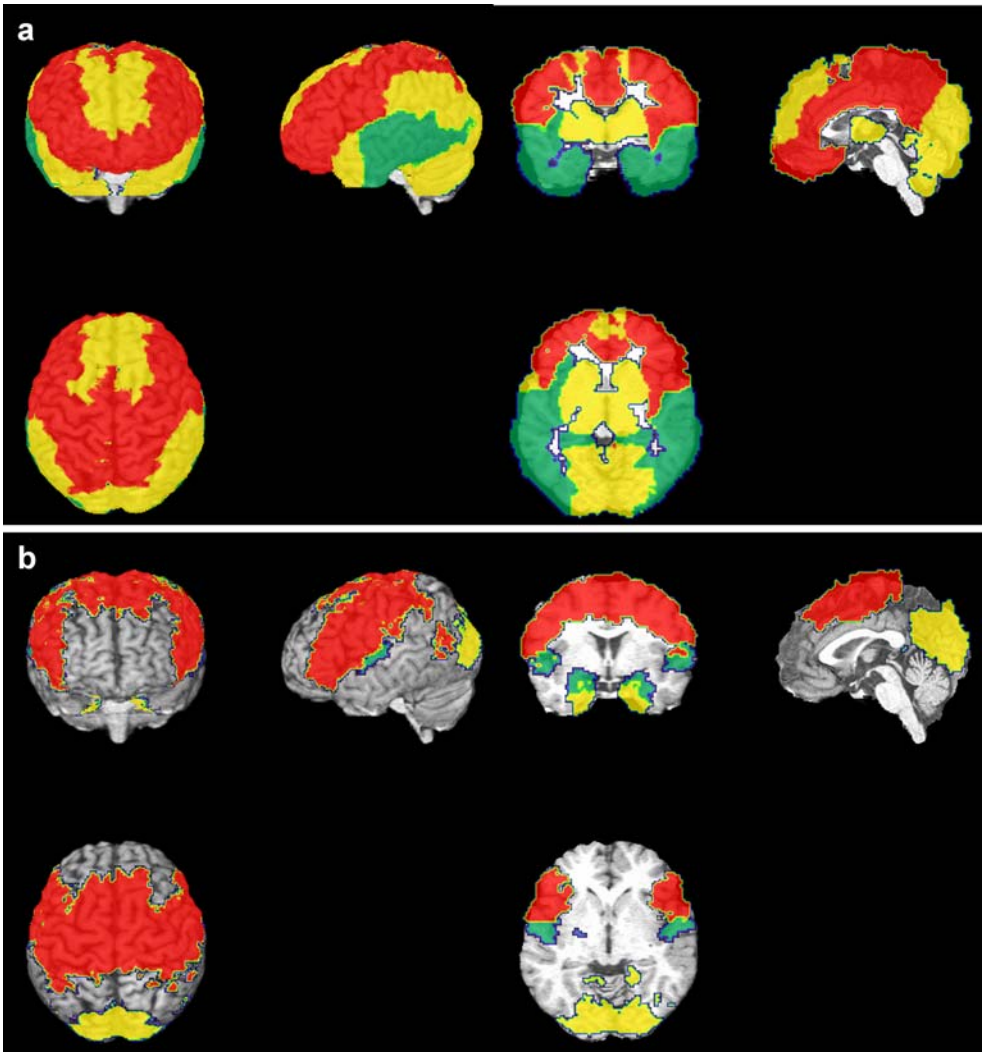

Fig. 4 **a** Spectrum of interregional correlation patterns of gyral VOIs. The figure shows patterns of correlation for 70 gyral VOIs, which ranged 'autocorrelation' to 'interregional correlation' with wider areas. **b** Spectrum of interregional correlation patterns for cytoarchitectonic VOIs. Patterns of correlation for 28 cytoarchitectonic VOIs ranged from 'autocorrelation' to 'interregional correlation' with wider areas. *Green* indicates autocorrelation and no interregional correlation with contralateral counterparts or adjacent areas, *yellow* indicates interregional correlation with contralateral counterparts and adjacent areas, and *red* interregional correlation with more distant regions

VOIs. Green depicts VOIs showing 'autocorrelation only', yellow VOIs showing correlations with contralateral homologues, and red VOIs showing additional correlation with wider areas.

Effect of seed VOI size or seed VOI defining-method on interregional correlation patterns

Seed VOI sizes ranged from 163 (globus pallidus) to 6,091 (middle frontal gyrus) voxels (Suppl. Table 1), and interregional correlations tended to be more confined for smaller size VOIs (Suppl. Fig. 7). Although sizes of seed VOI were similar (i.e., 2,000 to 4,000 voxels), their extent of interregional correlation varied widely from several thousand voxels (autocorrelation) to more than 10,000 voxels. When the size ratios of correlated regions were compared with seed VOI sizes, no correlation was found (Fig. 6).

Frontal, parietal, and occipital lobes showed bilateral correlations with respective seed lobes (Suppl. Fig. 6a and b). However, the interregional correlations of both temporal lobes tended to be confined to ipsilateral hemispheres (Suppl. Fig. 6b). When comparing patterns of correlated area extents, determined using gyral and cytoarchitectonic methods (Fig. 4a and b), no difference was found.

Discussion

In this connectivity study, anatomical localizers, i.e., lobes, gyri, and BA, were used to define VOIs in the brain, and IRCA/FDG-PET studies showed characteristic patterns of connectivity throughout lobes, gyri, and BA regardless of the VOI-define method used or VOI size. Autocorrelations were found for all seed VOIs, and correlations with contralateral homologues were found in two thirds of gyri, which concur with the findings of Horwitz et al. [13]. In the present study, we used a novel method using FDG-PET beside those used previously to examine default mode resting network. Single scans in each subject provided the opportunity to study resting connectivity in the normal

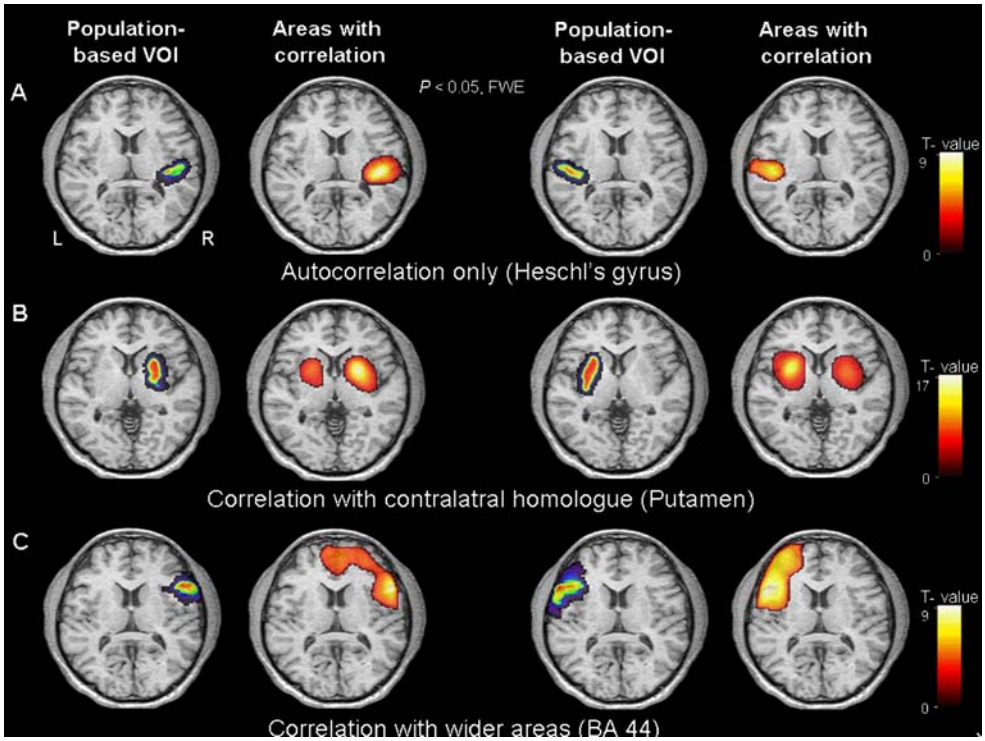

Fig. 5 Examples are showing three patterns of metabolic connectivity. Family-wise error correction ($P<0.05$). **a** Brain areas showing interregional correlation with FDG uptake by Heschl's gyri. Regions were confined to themselves and nearest adjacent areas. Note the absence of a correlation with counterparts in the contralateral hemisphere. The population-based VOIs of Heschl's gyri are shown in the top left most column. **b** Brain areas showing interregional correlation with putamen. Autocorrelation and correlations with contralateral counterparts were characteristic, and correlations were found with nonadjacent regions. Population-based VOIs of the putamen are shown in the *middle leftmost column*. **c** Correlations between BA44 were *widespread and even crossed midline*. The asymmetries of the correlation patterns of left and right BA44 regions were *prominent*. Areas correlated with right BA44 were *adjacent to the anterior medial parts of the VOI*, while those of the left BA44 were more confined to the *ipsilateral hemisphere*

adult human brain. The detection of autocorrelations for all seed VOIs (even small VOIs) implies that the recruited sample size ($n=50$) was sufficient for statistical purposes. Moreover, our analysis was based on the use of a corrected P value cutoff of 0.05, which we used in our previous study, which had a sample size of more than 100 [25]. In the present study, we were able to assess regional glucose consumption by brain FDG-PET, and we propose that interregional connectivity in metabolic terms can be assessed by FDG-PET objectively with satisfactory robustness.

Table 1 Spectrum of interregional correlation patterns for gyral VOIs

Autocorrelation	Interregional correlation with contralateral counterparts and adjacent or remote areas	
Amygdala	Cerebellum	Anterior cingulate gyrus
Hippocampus	Thalamus	Posterior cingulate gyrus
Parahippocampal gyrus	Putamen	Postcentral gyrus[a]
Planum polare	Caudate	Superior parietal gyrus
Heschl's gyrus	Globus pallidus	Precuneus
Planum temporale	Cuneus	Inferior frontal gyrus[a]
Superior temporal gyrus	Fusiform gyrus	Middle frontal gyrus[a]
Middle temporal gyrus	Lingual gyrus	Orbiotofrontal gyrus
Inferior temporal gyrus	Superior lateral occipital gyrus	Precentral gyrus[a]
Occipitotemporal gyrus	Supramarginal gyrus	Supplementary motor areas
Inferolateral occipital gyrus	Angular gyrus	Right insula[a]
Left insula[a]	Temporal pole	
	Superior frontal gyrus	

VOIs volumes of interest

[a] Denotes that right and left seed VOIs showed hemispheric asymmetry with respect to correlated regions.

Table 2 Spectrum of interregional correlation patterns for cytoarchitectonic VOIs

Autocorrelation	Interregional correlation with contralateral counterparts and adjacent or remote areas	
Amygdala	BA 1 (somatosensory cortex)	BA 44 (Broca's areas)[a]
BA 41 (primary auditory cotex)	BA 2 (somatosensory cortex)	BA 45 (Broca's areas)[a]
	BA 3 (primary somatosensory cortex)	V5[a]
	BA 4 (primary motor cortex)	
	BA 6 (premotor cortex)	
	BA 17 (visual areas V1)	
	BA 18 (visual areas V2)	
	Anterior intraparietal sulcus	
	Entorhinal cortex	

VOIs volumes of interest, *BA* Brodmann area

[a] Denotes that right and left seed VOIs showed hemispheric asymmetry with respect to correlated regions.

Methodological issues

The method of analysis used in the present study has been used previously to identify connectivities and their changes during the development of profound deaf subjects [25] and also to identify differential patterns of connectivity within various subareas of the posterior cingulate gyrus based on metabolic connectivity [26]. Both studies showed patterns of connectivity with seed VOIs defined using anatomical methods, and the authors considered that metabolic connectivity represented neuronal connectivity. We share this opinion. In our investigation, we initially used population-based VOIs developed in-house based on high-resolution MRI [17, 31]. Cytoarchitectonically defined VOIs added further confidence to our investigation, which suggested that patterns of interregional correlation are not simply due to arbitrary anatomical localizers.

Some gyri consist of many heterogeneous functional units, and even BAs have different functionalities associated with their specialties and varieties of interregional connections [26]. When sizes of correlated areas were plotted against sizes of seed VOIs, an apparent correlation was observed; that is, smaller seed VOIs were correlated with smaller areas (Suppl. Fig. 7). However, when the relation between size ratios, which represents the normalized extent of correlated areas with respect to seed VOI size, and seed VOI sizes was investigated, no discernible correlation was found. We suppose that patterns of connectivity rely predominantly on seed VOI location. When we compared extents of correlated area patterns for the two VOI-defining methods (i.e., gyral and cytoarchitectonic), no difference was found. Thus, interregional connectivity patterns appear to be unique to brain regions and not VOI size or VOI-defining method used.

Studies on the feasibilities of FDG-PET-based correlation studies led earlier investigators to search for patterns of brain connectivity at rest [13, 27–30], and strongest correlations were found between bilateral homologues, though strong correlations were also found between certain areas of frontal and parietal lobes [13]. In the present study, using anatomical localizers, voxel-based approaches, and appropriate visual displays, we were able to discern the patterns of interregional correlation for anatomical localizers and easily identify recognizable connectivity outputs. We concur with earlier studies that bilateral homologues had stronger interregional

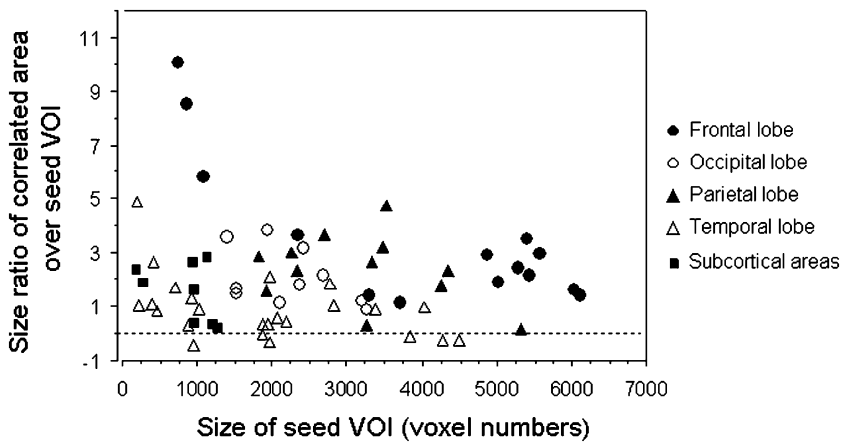

Fig. 6 Correlations between size ratios (sizes of correlated areas divided by corresponding seed VOI sizes) and seed VOI sizes. *Closed and open circles* and *closed and open triangles* indicate seed VOIs of frontal/occipital and parietal/temporal lobes. Note the *clustering of closed circles and closed triangles*, indicating that these seed VOIs of frontal and parietal lobes had larger correlated regions

correlations and that frontal/parietal lobes show extensive metabolic connectivity [13]. Specifically, areas defined in the present investigation were anatomical and based on population data, and thus, we were able to avoid post hoc arbitrariness or possible redundancy when using functional localizers [14, 16].

Pattern of metabolic connectivity

In this investigation, spectra of interregional correlations in normal adults were found to range from 'autocorrelation only' to 'widespread'. The present study produced three findings regarding metabolic connectivity in the brain. First, autocorrelation was observed for all seed VOIs. 'Autocorrelation' as used in the present study was not a trivial finding, as entire brain voxels were searched for possible correlations with mean counts of designated seed VOIs as determined by SPM. If VOI analysis findings (not voxels but VOIs themselves) were used instead of voxel-wise analysis for IRCA, self-correlations would have been obtained automatically regardless of the locations or sizes of seed VOIs. When we decreased the sample size to 12 from 50, no autocorrelation was observed for some seed VOIs. Furthermore, 'autocorrelation only' should not mean 'no connectivity', but that interregional correlations are confined to seed VOIs. We defined 'autocorrelation only' based on the hypothesis that all voxels in seed VOIs are related to the weighted mean counts of seed VOIs and that connectivity overflow did not reach any adjacent separate VOIs. 'Autocorrelation only' is characterized by its isolation and not to a lack of correlation. Temporal lobe VOIs tended to be more likely to show 'autocorrelation only', and 20 gyri that showed 'autocorrelation only' were mainly located in temporal lobes (Fig. 4); moreover, the absence of a connection to contralateral counterpart was found to be characteristic temporal lobes themselves (Suppl. Fig. 6b). Cytoarchitectonically defined primary auditory cortex and amygdala regions behaved similarly.

Second, correlated area extents were symmetric for the left and right homologues in most seed VOIs, except for a few seed VOIs, typically clustered near VOIs. While anatomical asymmetries of small magnitude were observed between both hemispheric VOIs in individual brains [24], we identified homologous VOIs in both hemispheres that showed definitive asymmetry in their connectivity patterns. These were the precentral and postcentral gyri, middle and inferior frontal gyri, and insula. Similar asymmetries were for BA44 and 45 and V5. The cognitive implications of interregional correlation symmetries and asymmetries for individual seed VOIs warrant further investigation.

The third characteristic pattern of adjacent/remote brain connectivity is well documented in certain brain regions and provokes great interest; it concerns widespread connectivities that sometimes cross the midline. In our previous study, we reported asymmetries of greater extent in the interregional correlation patterns of BA41 (primary auditory cortex), but this study was conducted in deaf children [25]. The present investigation revealed that there are extensive asymmetric connectivity patterns in some gyri of frontal or other lobes in normal humans, i.e., other than in the primary auditory cortex.

More than two thirds of gyral VOIs and most BA VOIs showed variable ranges of interregional correlation with adjacent or remote areas in addition to autocorrelation. Widespread correlation included 'connectivity with contralateral homologues' in most VOIs. Cerebellum, deep gray matters, cingulate gyri, frontal, parietal, and occipital gyri all showed connectivity with contralateral homologues (Fig. 4), which suggests that these anatomically defined areas are homologous in terms of their functional connectivities with contralateral counterparts. This connectivity with contralateral counterparts was reconfirmed by the similar characteristics of BA1, 2, 3, 4 (Suppl. Fig. 3), 6, 17, and 18, the anterior intraparietal sulcus, and V5. Of these areas, cingulate gyri, precentral and postcentral gyri, frontal and parietal gyri, and their counterpart BAs (i.e., 1, 2, 3, 4, 6) and the anterior intraparietal sulcus showed considerable widespread connectivity. BA44 (Suppl. Fig. 5) and 45 provide good examples because they show extensive connectivity with adjacent areas and little connectivity with contralateral homologues. The connectivities of bilateral V5/MT were also characterized by their far-reaching connectivities with auditory and visual cortices. Moreover, the connectivities of right V5/MT were symmetric in terms of their spatial distributions, whereas those of left V5/MT were more dominant in the left hemisphere.

Metabolic connectivity vs. anatomical or neural connectivities

Interregional correlations between normative areas by FDG-PET revealed that metabolic connectivity did not exactly reflect anatomical connectivity defined either by white matter connectivity on diffusion tensor imaging (DTI) or that speculated based on primate connectivity. Noninvasive DTI [32] and histochemical axon-connection [33] analyses cannot produce the information generated by the present study, though they provide valuable information concerning the hardwired aspect of functional connectivity. In contrast to the hardwiring of brain areas, metabolic functional connectivity is supposed to represent metabolic soft-wiring of brain areas like fMRI or water PET. By examination of glucose metabolic activity in the brain and scrutinizing the interregional correlations of these activities, we believe that information 'traffic' can be examined on the anatomical 'roads' present in the brain.

Regional connections as determined by FDG-PET are now better understood. According to recent magnetic resonance spectroscopic studies [34–36] on FDG-PET, neuronal activities are reflected by neuronal oxidative glucose metabolism, which is linearly correlated with glutamine–glutamate cycling, despite complex interplay between neurons and astrocytes [35–40]. Astrocytes take up glucose and shuttle lactate to neurons, which finally oxidize lactate and glucose [37–40]. In terms of the sequential coupling of neuronal activity, metabolism, and perfusion, regional metabolic connections might precede regional blood flow connections, as visualized by water PET or fMRI, and represent neuronal connectivities between brain areas. In this sense, default mode fMRI and water PET studies might be complemented by interregional correlative FDG-PET studies. FDG-PET has lower temporal resolution than water PET or fMRI. This resolution is of the order of tens of minutes to an hour, and thus, metabolic activity information represents brain in steady state in hourly terms. In brief, brain metabolic functional connectivity examined by FDG-PET represents the basal state and is mainly excitatory (excitatory to inhibitory ratio 4 to 1) and neuronal (neuronal to astrocytic 85% to 15%) and mostly synaptic [34, 37–41].

When fMRI or water PET are used to study at rest cognitive tasks, subjects might use default mode brain circuitry at various levels of mental loads and/or recruit other systems unique to relevant tasks. Uniquely using IRCA/FDG-PET, we were able to detect steady-state metabolic connectivities and their variations in drifting states, and thus, we believe that disease-specific changes of interregional brain circuitry correlations will be disclosed during further investigations. However, to establish this, individual variations should be within statistical subject-to-subject variations. Patterns of default-mode connectivity differ between individuals. However, based on a recent observation [42], we are able to hypothesize that humankind is adequately represented by statistically meaningful variations in single FDG-PET images of individuals [25, 26]. Moreover, the availability of norms of metabolic connectivity by IRCA FDG-PET would allow meaningful studies of abnormalities associated with default metabolic connectivities.

Summary

In the present study, we found characteristic patterns of interregional correlation by examining the metabolic activities of normative areas in the normal adult human brain. Our findings are presented in a descriptive fashion to give the reader an overview of default metabolic functional connectivities in the normal human brain. Typical patterns were autocorrelation, connectivity with contralateral homologues, and connectivity with extensive and sometimes asymmetric adjacent/remote areas. We propose that this basal metabolic connectivity of brain regions should be taken into account when attempts are made to understand metabolic connectivity abnormalities associated with disease or changes associated with development or aging.

Acknowledgments This study was supported by the Brain Research Center of the 21st Century Brain Frontier Project of the Korean Ministry of Science (M103KV010017-07K2201-01710), by the Korean Science and Engineering Foundation (KOSEF), and by the Korean Ministry of Science and Technology (MOST) through its National Nuclear Technology Program (#M20504070004-05A0707-00410). We deeply appreciate the efforts of Professors Zilles and Amunts for transferring their Brodmann Areas to Korean templates. This study utilized KREONET (the Korean Research Network) a Giga-bps high speed network.

References

1. Raichle ME, MacLeod AM, Snyder AZ, Powers WJ, Gusnard DA, Shulman GL. A default mode of brain function. Proc Natl Acad Sci U S A 2001;98:676–82.
2. Greicius MD, Krasnow B, Reiss AL, Menon V. Functional connectivity in the resting brain: a network analysis of the default mode hypothesis. Proc Natl Acad Sci U S A 2003;100:253–8.
3. De Luca M, Beckmann CF, De Stefano N, Matthews PM, Smith SM. fMRI resting state networks define distinct modes of long-distance interactions in the human brain. Neuroimage 2006;29:1359–67.
4. Rissman J, Gazzaley A, D'Esposito M. Measuring functional connectivity during distinct stages of a cognitive task. Neuroimage 2004;23:752–63.
5. Rombouts SA, Stam CJ, Kuijer JP, Scheltens P, Barkhof F. Identifying confounds to increase specificity during a "no task condition". Evidence for hippocampal connectivity using fMRI. Neuroimage 2003;20:1236–45.
6. Lahaye PJ, Poline JB, Flandin G, Dodel S, Garnero L. Functional connectivity: studying nonlinear, delayed interactions between BOLD signals. Neuroimage 2003;20:962–74.
7. van de Ven VG, Formisano E, Prvulovic D, Roeder CH, Linden DE. Functional connectivity as revealed by spatial independent component analysis of fMRI measurements during rest. Hum Brain Mapp 2004;22:165–78.
8. Horwitz B, Braun AR. Brain network interactions in auditory, visual and linguistic processing. Brain Lang 2004;89:377–84.
9. Esposito F, Bertolino A, Scarabino T, Latorre V, Blasi G, Popolizio T, et al. Independent component model of the default-mode brain function: Assessing the impact of active thinking. Brain Res Bull 2006;70:263–9.
10. Fransson P. How default is the default mode of brain function? Further evidence from intrinsic BOLD signal fluctuations. Neuropsychologia 2006;44:2836–45.
11. Horwitz B. The elusive concept of brain connectivity. Neuroimage 2003;19:466–70.
12. Lee L, Harrison LM, Mechelli A. A report of the functional connectivity workshop, Dusseldorf 2002. Neuroimage 2003;19:457–65.
13. Horwitz B, Duara R, Rapoport SI. Age differences in intercorrelations between regional cerebral metabolic rates for glucose. Ann Neurol 1986;19:60–7.
14. Friston KJ, Rotshtein P, Geng JJ, Sterzer P, Henson RN. A critique of functional localisers. Neuroimage 2006;30:1077–87.

15. Penny WD, Stephan KE, Mechelli A, Friston KJ. Modeling functional integration: a comparison of structural equation and dynamic causal models. Neuroimage 2004;23(Suppl 1):S264–2S74.
16. Saxe R, Brett M, Kanwisher N. Divide and conquer: a defense of functional localizers. Neuroimage 2006;30:1088–96.
17. Lee JS, Lee DS. Analysis of functional brain images using population-based probabilistic atlas. Curr Med Imag Rev 2005;1:81–7.
18. Kim JJ, Crespo-Facorro B, Andreasen NC, O'Leary DS, Zhang B, Harris G, et al. An MRI-based parcellation method for the temporal lobe. Neuroimage 2000;11:271–88.
19. Amunts K, Zilles K. Advances in cytoarchitectonic mapping of the human cerebral cortex. Neuroimaging Clin N Am 2001;11:151–69.
20. Lee JS, Lee DS, Kim YK, Kim JS, Lee JM, Koo BB, et al. Quantification of brain images using Korean standard templates and structural and cytoarchitectonic probabilistic maps. J Korean Nucl Med 2004;38:241–52.
21. Waites AB, Briellmann RS, Saling MM, Abbott DF, Jackson GD. Functional connectivity networks are disrupted in left temporal lobe epilepsy. Ann Neurol 2006;59:335–43.
22. Amunts K, Malikovic A, Mohlberg H, Schormann T, Zilles K. Brodmann's areas 17 and 18 brought into stereotaxic space-where and how variable. Neuroimage 2000;11:66–4.
23. Morosan P, Rademacher J, Schleicher A, Amunts K, Schormann T, Zilles K. Human primary auditory cortex: cytoarchitectonic subdivisions and mapping into a spatial reference system. Neuroimage 2001;13:684–701.
24. Amunts K, Schleicher A, Burgel U, Mohlberg H, Uylings HB, Zilles K. Broca's region revisited: cytoarchitecture and intersubject variability. J Comp Neurol 1999;412:319–41.
25. Kang E, Lee DS, Lee JS, Kang H, Hwang CH, Oh SH, et al. Developmental hemispheric asymmetry of interregional metabolic correlation of the auditory cortex in deaf subjects. Neuroimage 2003;19:777–83.
26. Vogt BA, Vogt L, Laureys S. Cytology and functionally correlated circuits of human posterior cingulate areas. Neuroimage 2006;29:452–66.
27. Horwitz B, Duara R, Rapoport SI. Intercorrelations of glucose metabolic rates between brain regions: application to healthy males in a state of reduced sensory input. J Cereb Blood Flow Metab 1984;4:484–99.
28. Horwitz B, Rumsey JM, Grady CL, Rapoport SI. The cerebral metabolic landscape in autism. Intercorrelations of regional glucose utilization. Arch Neurol 1988;45:749–55.
29. Horwitz B, Schapiro MB, Grady CL, Rapoport SI. Cerebral metabolic pattern in young adult Down's syndrome subjects: altered intercorrelations between regional rates of glucose utilization. J Ment Defic Res 1990;34:237–52.
30. Horwitz B, Swedo SE, Grady CL, Pietrini P, Schapiro MB, Rapoport JL, et al. Cerebral metabolic pattern in obsessive-compulsive disorder: altered intercorrelations between regional rates of glucose utilization. Psychiatry Res 1991;40:221–37.
31. Lee JS, Lee DS, Kim J, Kim YK, Kang E, Kang H, et al. Development of Korean standard brain templates. J Korean Med Sci 2005;20:483–8.
32. Johansen-Berg H, Behrens TE, Robson MD, Drobnjak I, Rushworth MF, Brady JM, et al. Changes in connectivity profiles define functionally distinct regions in human medial frontal cortex. Proc Natl Acad Sci USA 2004;101:13335–40.
33. Schmahmann JD, Pandya DN. Fiber pathways of the brain. Oxford University Press: New York; 2006.
34. Shulman RG, Rothman DL. Brain energetics and neuronal activity. Wes Sussex, England: Wiley and Sons Ltd; 2004.
35. Hertz L, Zielke HR. Astrocytic control of glutamatergic activity: astrocytes as stars of the show. Trends Neurosci 2004;27:735–43.
36. Gruetter R, Adriany G, Choi IY, Henry PG, Lei H, Oz G. Localized in vivo 13C NMR spectroscopy of the brain. NMR Biomed 2003;16:313–38.
37. Pellerin L. How astrocytes feed hungry neurons. Mol Neurobiol 2005;32:59–2.
38. Hyder F, Patel AB, Gjedde A, Rothman DL, Behar KL, Shulman RG. Neuronal-glial glucose oxidation and glutamatergic–GABAergic function. J Cereb Blood Flow Metab 2006;26:865–77.
39. Magistretti PJ. Neuron-glia metabolic coupling and plasticity. J Exp Biol 2006;209:2304–11.
40. Magistretti PJ, Pellerin L. Cellular mechanisms of brain energy metabolism and their relevance to functional brain imaging. Philos Trans R Soc Lond B Biol Sci 1999;354:1155–63.
41. Behar KL, Rothman DL. NMR studies of the metabolism and energetics of GABA neurotransmitter pathways. In: Shulman RG, Rothman DL, editors. Brain energetics and neuronal activity. West Sussex, England: Wiley; 2004. p. 100–1.
42. Damoiseaux JS, Rombouts SA, Barkhof F, Scheltens P, Stam CJ, Smith SM, et al. Consistent resting-state networks across healthy subjects. Proc Natl Acad Sci U S A 2006;103:13848–53.
43. Geyer S, Schleicher A, Zilles K. Areas 3a, 3b, and 1 of human primary somatosensory cortex. Neuroimage 1999;10:63–3.
44. Grefkes C, Geyer S, Schormann T, Roland P, Zilles K. Human somatosensory area 2: observer-independent cytoarchitectonic mapping, interindividual variability, and population map. Neuroimage 2001;14:617–31.
45. Amunts K, Jancke L, Mohlberg H, Steinmetz H, Zilles K. Interhemispheric asymmetry of the human motor cortex related to handedness and gender. Neuropsychologia 2000;38:304–12.
46. Malikovic A, Amunts K, Schleicher A, Mohlberg H, Eickhoff SB, Wilms M, et al. Cytoarchitectonic analysis of the human extrastriate cortex in the region of V5/MT+: a probabilistic, stereotaxic map of area hOc5. Cereb Cortex 2007;17:562–74.
47. Caspers S, Geyer S, Schleicher A, Mohlberg H, Amunts K, Zilles K. The human inferior parietal cortex: cytoarchitectonic parcellation and interindividual variability. Neuroimage 2006;33:430–48.
48. Amunts K, Kedo O, Kindler M, Pieperhoff P, Mohlberg H, Shah NJ, et al. Cytoarchitectonic mapping of the human amygdala, hippocampal region and entorhinal cortex: intersubject variability and probability maps. Anat Embryol (Berl) 2005;210:343–52.